

Original Article

DOI 10.1007/s12206-023-0305-0

Keywords:

- Center of gravity adjustment system
- Dynamics analysis
- PID control
- Control system stability

Correspondence to:

Chul-Hee Lee  
chulhee@inha.ac.kr

Citation:

Jiang, Z., Lee, C.-H. (2023). Design of personal mobility system for assisted agricultural work with self-adjusting center of gravity. *Journal of Mechanical Science and Technology* 37 (4) (2023) 1623~1635. <http://doi.org/10.1007/s12206-023-0305-0>

Received June 22nd, 2022

Revised October 18th, 2022

Accepted December 26th, 2022

† Recommended by Editor  
No-cheol Park

# Design of personal mobility system for assisted agricultural work with self-adjusting center of gravity

Zixuan Jiang and Chul-Hee Lee

Department of Mechanical Engineering, Inha University, Incheon 22212, Korea

**Abstract** A personal mobility system with a self-adjusting center of gravity is designed to aid agricultural work. This personal mobility system can assist elderly and disabled people with mobility problems to perform simple agricultural tasks. Simulations and experiments were performed using a 2.5-times reduced model of the personal mobility system, and the feasibility and effectiveness of the proposed system were verified. With the initial position of the center of gravity of the personal mobility system as the set value, the proportional-integral-derivative control of the counterweight motion is coordinated horizontally using two corresponding motors and the center of gravity of the system is controlled within a certain range of the set value. The experimental transition time is 10.8 s and the simulated transition time is 10.4 s. The error between the two is 3.85 %. The results demonstrate that the proposed adaptive control system achieves adaptive adjustment of the center of gravity.

## 1. Introduction

The World Health Organization (WHO) estimates that there are approximately one billion people with disabilities worldwide. Eighty percent of these people live in developing countries. According to the results of a sample survey, there are approximately 24.72 million people with physical disabilities, of which the number of people with lower-limb disabilities accounts for approximately 70 % [1]. Many elderly people are unable to walk as a result of reduced function of their lower extremities caused by declining physical fitness or long-term bedrest. Personal mobility systems are an important research area focused on developing service robot products for the disabled and elderly [2].

With the advancements in artificial intelligence and big data technologies, the development of personal mobility systems is progressing rapidly. The basis of most personal mobility systems is the electric wheelchair, and intelligent technologies are typically added to existing electric wheelchairs to provide additional functionality [3]. Foreign-produced personal mobility systems are expensive and difficult for most people with disabilities to afford. These excessively high costs make such systems a poor choice for the average farming family. The operation of ordinary wheelchairs that are available on the market requires a high level of physical mobility, resulting in people with physical deficits being unable to operate and control their wheelchairs autonomously; this obligates such people to seek assistance of a guardian to accomplish the effective operational control of a wheelchair [4]. Although several domestic companies produce electric wheelchairs, the development of their control systems is still in the early stages and their control parameters are limited. Consequently, they cannot fully meet the needs of people with disabilities in daily life [5]. The development of an agricultural assistance personal mobility system that is safe, reliable, and practical can significantly improve the quality of daily life and work of disabled and elderly people, helping them take care of themselves, compensating for a lack of physical function, and enabling their reintegration into society. Involving the elderly and disabled who can work in labor can address the economic needs of farming families while ensuring the mobility and self-reliance of the disadvantaged in their daily lives and alleviating their

survival anxiety. Moreover, providing them full access to outdoor activities will improve their quality of life.

A personal mobility system is designed based on a conventional manual wheelchair equipped with a high-performance power drive, intelligent manipulation devices, batteries, and other components that can be transformed and upgraded. The manual manipulation of an intelligent controller can drive a personal mobility system to complete a variety of functions such as moving forward and backward, steering, standing, and lying down. Such high-tech products involve modern precision machinery, intelligent numerical control, engineering mechanics, and other fields [6-11].

Several studies have focused on personal mobility systems. Akira Sasou from Australia proposed a human-machine interface approach to control an intelligent wheelchair based on head orientation assisted by sound [12]. The Smart Lab at MIT in the U.S.A. developed a semi-autonomous wheelchair robot called "Wellesley" that is equipped with multiple sensors and controlled by a computer in real time [13]. The RIKEN BSI-Toyota Collaboration Center in Japan has developed a motorized-wheelchair-controlled system in which the rider wears a brainwave detection device and can successfully operate the wheelchair with more than 95 % reliability by visualizing movement in three directions corresponding to forward, left rotation, and right rotation, as well as movement away from the left and right arms [14].

Additionally, ordinary manual and intelligent wheelchairs can be upgraded to power-assisted-control wheelchairs [15]. For wheelchair riders, Cooper et al. of the University of Pittsburgh [16] proposed a manually activated form of assisted-power-driven wheelchair that automatically controls the torque of the drive motor by adjusting the power output in proportion to the force applied by an occupant to the wheelchair spokes. This compensates for the deficiencies in ordinary wheelchairs that rely on pure human power. Seki et al. [17-19] of the Chiba Institute of Technology conducted a series of related studies based on Yamaha's JW II power-assisted wheelchairs. Personal mobility systems also provide physical support and guidance, can and monitor the basic vital signs of users [20].

In this study, a personal mobility system for assisted agricultural work with a self-adjusting center of gravity was developed for people with disabilities and labor needs. First, a center of gravity adjustment system was designed based on an existing personal mobility system [21]. To verify the feasibility of the proposed design, a three-dimensional model of a personal mobility system for assisted agricultural work with a self-adjusting center of gravity was developed using multibody dynamics software. On this basis, simulations of the center of gravity self-adjustment of the personal mobility system for assisted agricultural work were performed for different rotation angles and forward speeds of the seat of the personal mobility system while carrying a person. Specifically, co-simulations were performed using a multibody dynamics software and Matlab Simulink. Finally, based on the results of the simulations, an experimental model with an equal-scale reduction of

2.5 times was constructed and several sets of experiments were conducted. By comparing the simulation and experimental data with the proportional-integral-derivative (PID) control quality index of the experimental center of gravity adjustment system as a reference, the feasibility of the design was verified and the control effect of the center of gravity self-adjustment system was evaluated.

The purpose of this paper is to verify the feasibility of self-regulation of the center of gravity of this personal mobility system for assisted agricultural work with self-adjusting center of gravity.

## 2. System modeling and kinematic dynamics analysis

### 2.1 Three-dimensional modeling

To reduce the time and cost requirements associated with experiments, a 2.5-times reduced scale model was used for both simulations and experiments. The personal mobility system for assisted agricultural work with a self-adjusting center of gravity was modeled in 3D using a multibody dynamics software.

In the study of a kinetic analysis system, primary and secondary factors often affect the mechanical properties of the study target. Typically, the focus is on the components or moving parts that have a major influence on the physical properties of the study target, and other components that have little or no influence on the kinematic properties of the analysis target are simplified. Therefore, the obtained analysis results do not affect the engineering requirements, but can account for the cost and demand.

Performing Boolean operations on parts that have no relative motion and are of the same type of material simplifies the material definition and constraint addition. The proposed personal mobility system is divided into seven parts, as shown in Fig. 1.

A newly developed model has no parameter information, so

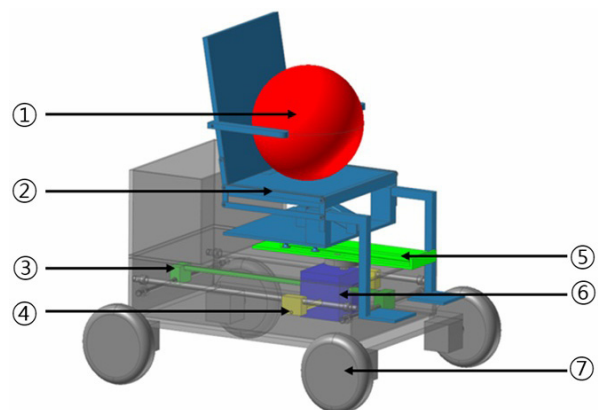


Fig. 1. Components of personal mobile systems (① model of simulated human body; ② seats; ③ Y-axis and slider; ④ X-axis and slider; ⑤ slide rail; ⑥ counterweight; ⑦ wheels, frame, and cargo box).

Table 1. Parameters of the personal mobile system.

Part	Mass (kg)	Moment of inertia (kg·m <sup>2</sup> )		
		lxx	lyy	lzz
①	5.12	1.843	1.843	1.843
②	0.64	6.938	5.845	2.558
③	0.1	2.098	2.098	1.003
④	0.08	7.453	7.44	9.704
⑤	0.512	2.543	2.423	1.3
⑥	3.2	2.129	2.129	2.121
⑦	9	0.377	0.252	0.188

such information must be defined by the user. By right-clicking on all the parts to modify their parameters, we selected geometry and material types. Because the materials of the parts of the personal mobility system for assisted agricultural work with a self-adjusting center of gravity were mainly various types of aluminum alloys, the material properties and density values were similar. Therefore, the material type of most of the structures was set to an aluminum alloy. The seat was set to a wood material and the tires were set to rubber materials.

After selecting appropriate materials, the mass characteristics of the parts, including their mass, rotational inertia, and other parameters, were obtained (Table 1).

## 2.2 Dynamic equations

Multibody dynamics is the study of multiple rigid or flexible bodies connected to each other under certain constraints and subjected to relative motion. Constraint types include incomplete, constant, and non-constant constraints. Multibody dynamics can be classified into multi-stiff-body dynamics and multi-flexible-body dynamics depending on whether a model contains flexible bodies. When the speed of motion or rotation of a moving system is low and its forces have little effect on deformation, it can be considered a multi-rigid-body. Otherwise, it is necessary to make the main moving parts of the system flexible. Contrary to Newton's law, Euler's equation, and Lagrange's equation, Kane's method does not require kinetic energy or potential energy, which can reduce calculation complexity and improve efficiency.

The Cartesian coordinate system of the center of mass of the rigid body and Euler angles reflecting the orientation of the rigid body are used as generalized coordinates and defined as

$$\begin{aligned} q &= [x, y, z, \psi, \theta, \phi]^T; \\ \text{make } R &= [x, y, z]^T; \\ \gamma &= [\psi, \theta, \phi]^T; \\ q &= [R^T, \gamma^T]^T. \end{aligned} \quad (1)$$

The coordinate transformation matrix between the reference coordinate system of the center of mass of the mechanical system components and ground coordinate system is

$$A^{\text{gl}} = \begin{bmatrix} A_{11} & A_{12} & A_{13} \\ A_{21} & A_{22} & A_{23} \\ A_{31} & A_{32} & A_{33} \end{bmatrix};$$

$$\begin{aligned} A_{11} &= \cos \psi \cos \phi - \sin \psi \cos \theta \sin \phi; \\ A_{12} &= -\cos \psi \sin \phi - \sin \psi \cos \theta \cos \phi; \\ A_{13} &= \sin \psi \sin \theta; \\ A_{21} &= \sin \psi \cos \phi + \cos \psi \cos \theta \sin \phi; \\ A_{22} &= -\sin \psi \sin \phi + \cos \psi \cos \theta \cos \phi; \\ A_{23} &= -\cos \psi \sin \theta, A_{31} = \sin \theta \sin \phi; \\ A_{32} &= \sin \theta \cos \phi, A_{33} = \cos \theta. \end{aligned} \quad (2)$$

An Euler rotation coordinate system is defined, where each of the above three Eulerian rotation axes has a vector of three units. Therefore, these three axes are not perpendicular to each other. The coordinate transformation matrix from this coordinate system to the component center of mass coordinate system is

$$B = \begin{bmatrix} \sin \theta \sin \phi & 0 & \cos \theta \\ \sin \theta \cos \phi & 0 & -\sin \theta \\ \cos \theta & 0 & 1 \end{bmatrix}. \quad (3)$$

The angular velocity of a component is expressed as:

$$\omega = B\gamma. \quad (4)$$

The variable  $\omega_e$  is introduced as a component of the angular velocity in the Euler rotational coordinate system, as follows:

$$\omega_e = \gamma. \quad (5)$$

Considering the constraint equations, the kinetic equations of the system are obtained using the energy form of the first Lagrange equation with Lagrange multipliers, as follows:

$$\frac{d}{dt} \left( \frac{\partial T}{\partial \dot{q}_j} \right) - \frac{\partial T}{\partial q_j} = Q_j + \sum_{i=1}^{i-1} \lambda_i \frac{\partial \phi_i}{\partial q_j}. \quad (6)$$

Here,  $T$  is the kinetic energy expressed in the generalized coordinates of the system,  $q_j$  represents the generalized coordinates,  $Q_j$  is the generalized force in the direction of  $q_j$ , and the final term represents the constraint equations and Lagrange multipliers expressing the constraint inverse force in the direction of the generalized coordinate. Generalized momentum  $P_j$  is introduced as follows:

$$P_j = \frac{\partial T}{\partial \dot{q}_j}. \quad (7)$$

The simplified expression for the constrained reaction force is

$$C_j = \sum_{i=1}^n \lambda_i \frac{\partial \phi}{\partial q_j} \tag{8}$$

Thus, Eq. (6) simplifies to

$$P_j - \frac{\partial T}{\partial q_j} = Q_j - C_j \tag{9}$$

The kinetic energy is expressed as

$$T = \frac{1}{2} R^T M R + \frac{1}{2} \gamma^T B^T J B \gamma \tag{10}$$

where  $M$  is the mass array of the member and  $J$  is the inertia array of the member in the center of mass coordinate system. According to the directions of motion and rotation.

$$P_R - \frac{\partial T}{\partial q_R} = Q_R - C_R \tag{11}$$

$$P_\gamma - \frac{\partial T}{\partial q_\gamma} = Q_\gamma - C_\gamma \tag{12}$$

Of which:

$$P_R = \frac{d}{dt} \left( \frac{\partial T}{\partial q_R} \right) = \frac{d}{dt} (MR) = MV, \quad \frac{\partial T}{\partial q_R} = 0 \tag{13}$$

This equation is simplified as

$$MV = Q_R - C_R \tag{14}$$

$$P_\gamma = \left( \frac{\partial T}{\partial q_\gamma} \right) = B^T J B \gamma \tag{15}$$

$B$  contains Euler angles, which are not derived further in  $P_\gamma$  to simplify derivation, but are solved as variables. This yields the following variables and equations for each building block.

$$\left. \begin{aligned} V &= [V_x, V_y, V_z]^T \\ R &= [x, y, z]^T \\ P_\gamma &= [P_\psi, P_\theta, P_\phi]^T \\ \omega_e &= [\omega_\psi, \omega_\theta, \omega_\phi]^T \\ \gamma &= [\psi, \theta, \phi]^T \end{aligned} \right\} \tag{16}$$

$$\left. \begin{aligned} MV &= Q_R - C_R \\ V &= R \\ P_\gamma - \frac{\partial T}{\partial q_\gamma} &= Q_\gamma - C_\gamma \\ P_\gamma &= B^T J B \omega_e \\ \omega_e &= \gamma \end{aligned} \right\} \tag{17}$$

We integrate these constraint equations to establish the differential algebraic equations for the dynamics of the system, yielding the following solution:

$$\left. \begin{aligned} P - \frac{\partial T}{\partial q} + \phi_q^T \lambda + H^T F &= 0 \\ P &= \frac{\partial T}{\partial q} \\ u &= q \\ \phi(q, t) &= 0 \\ F &= f(u, q, t) \end{aligned} \right\} \tag{18}$$

where  $P$  is the generalized momentum of the system and  $H$  is the coordinate transformation matrix for the external forces [22].

The PID control equation is

$$u = k_p e + k_i \int_0^t e dt + k_d \dot{e} \tag{19}$$

The expression for parameter self-adjustment is

$$k_p + k_i \frac{1}{s} + k_d \frac{N}{1 + N \frac{1}{s}} = 0 \tag{20}$$

where  $e$  is deviation of the measured value from the set value.  $k_p$  is proportionality coefficient,  $k_i$  is integral coefficient,  $k_d$  is differential coefficient.  $N$  is filter parameters.  $S$  is Laplace operator.

### 3. Co-simulation analysis based on multi-body dynamics software and Matlab

#### 3.1 Constraints and drivers of the simulation model

A translation joint was added between the seat and slide, fixed joint was added between the slide and rotating gear, revolute joint was added between the rotating gear and center of the gravity adjustment device, moving vice was added between the counterweight and shaft, and translate joint was added between the slider and shaft. Additionally, no relative motion is considered between the wheel and earth. Therefore, a fixed joint was added between the wheel and earth. Two translation forces denoted as  $F_x$  and  $F_y$  were applied to the counterweight along the X and Y axes, respectively. The dynamic model after adding the constraints and drivers is presented in Fig. 2. We defined  $F_x$  and  $F_y$  as the outputs and the X and Y coordinates of the center of gravity as the inputs.

#### 3.2 The control section of the co-simulation

Based on mechanical system simulations, the co-simulation process for the system was designed using co-simulations of multibody dynamics and Matlab Simulink, and a simulation

Table 2. Self-adjusting parameters of the PID controller module.

Proportional (P)	10
Integral (I)	1
Derivative (D)	25
Filter coefficient (N)	100

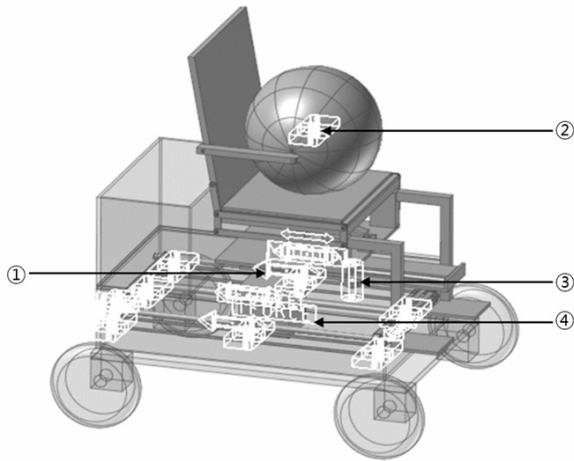


Fig. 2. Joint and force of the simulation model (① translate joint; ② fixed joint; ③ revolute joint; ④ translation force).

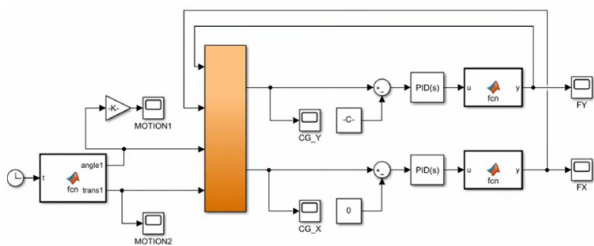


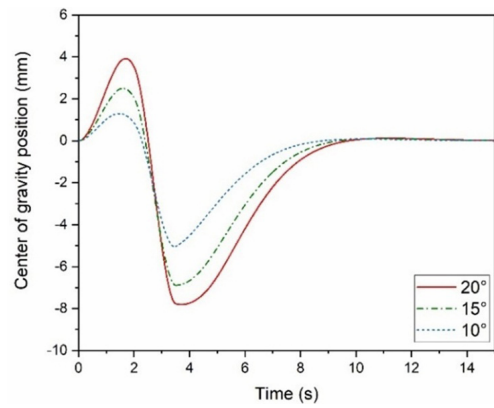
Fig. 3. Simulation module in Simulink.

module for the center of gravity adjustment system was established, including a PID controller for performing adjustment. The SIMULINK simulation module is shown in Fig. 3.

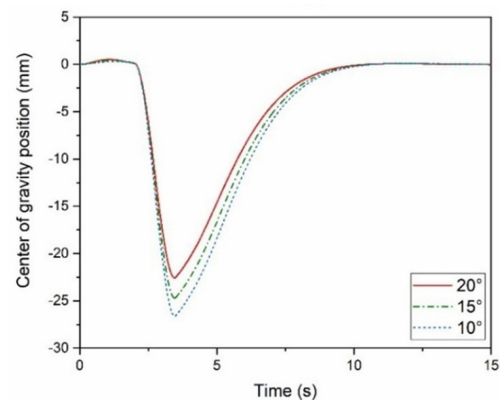
By self-adjusting the control parameters, the center of gravity of the personal mobility system, designed for assisted agricultural work, can be adjusted during seat movement. The self-adjusting PID controller module settings are listed in Table 2.

Considering that the motor speed and response speed are too fast for real-world experiments, which would lead to system oscillation and control instability, a maximum output limit was also defined in the simulations to enable comparisons with the experimental data.

The movements that can cause the center of gravity to change when the personal mobility system is used to assist in agricultural operations include the rotation, and forward and backward movements of the seat, change in posture of the seat, increase and decrease in cargo weight in the cargo box, and body movements of the driver. The seat rotates and then moves forward, causing the center of gravity of the personal



(a)



(b)

Fig. 4. Results of the center of gravity position of in the simulations for different rotation angles of the seat: (a) movement along the X axis; (b) movement along the Y axis.

mobility system to change significantly in a short period. Therefore, the motion caused by the rotation and forward movement of the seat was selected for comparing the simulation and experimental data on the self-adjustment of the center of gravity of the personal mobility system to verify the feasibility of its design.

### 3.3 Results of the simulation

In the first set of simulation tests, the seat rotation angles were 20°, 15°, and 10°. The forward movement distance of the seat was 120 mm and the forward speed was 80 mm/s.

Fig. 4 presents the results for the center of gravity for different rotation angles of the seat in the first group of tests. The larger the rotation angle of the seat, the larger the offset of the center of gravity of the personal mobility system along the X axis and the smaller the offset along the Y axis. This is because different rotation angles result in different vectors of seat displacement along the X and Y axes. The larger the rotation angle of the seat, the larger the vector of the seat displacement along the X axis and the smaller the vector along the Y axis. Fig. 5 presents the results of the simulations for different seat rotation angles.

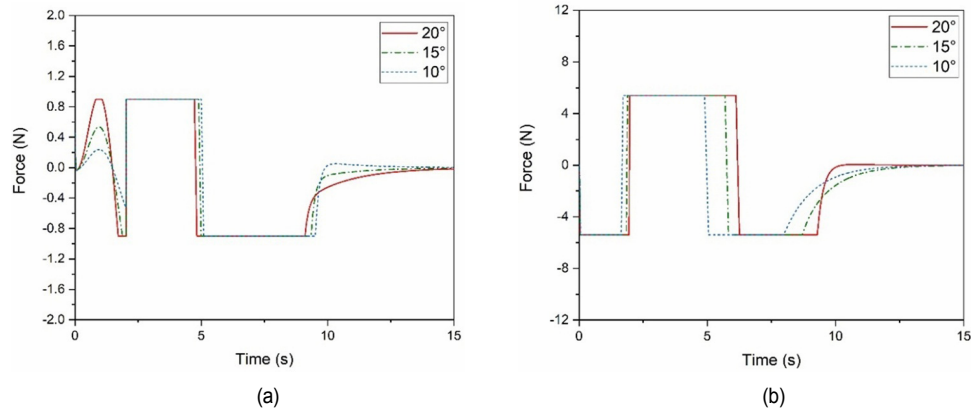


Fig. 5. Results of the output of simulations for different rotation angles of the seat: (a) movement along the X axis; (b) movement along the Y axis.

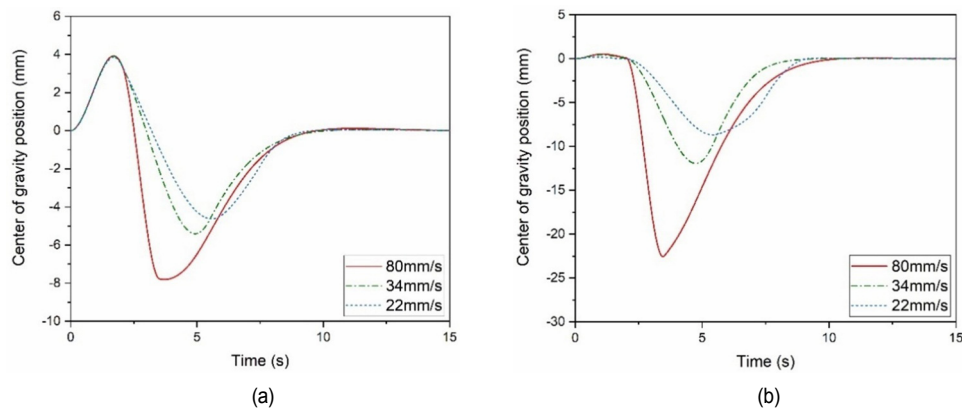


Fig. 6. Results of the center of gravity position in the simulations for different forward speeds of the seat: (a) movement along the X axis; (b) movement along the Y axis.

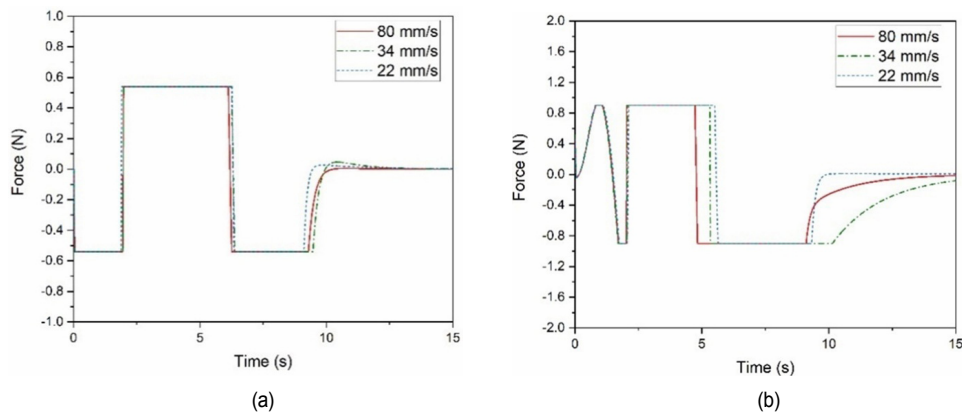


Fig. 7. Results of the output position of in the simulations for different advance forward speeds of the seat: (a) movement along the X axis; (b) movement along the Y axis.

The second group of variables focused on the forward speed of the simulation. The rotation angle of the seat was set  $20^\circ$  and the forward distance was set to 120 mm. The forward speed was varied between 80, 34, and 22 mm/s.

Fig. 6 presents the results for the center of gravity position in the simulations for different forward speeds of the seat in the second set of tests. The faster the seat advances, the greater the shift in the center of gravity of the personal mobility system

along the X and Y axes. Because the smaller the seat movement speed, the greater the offset of the center of gravity offset by the counterweight movement during the time the seat is moving. Fig. 7 presents the simulation results of the output positions for different forward seat speeds.

The simulation results show the offset in the center of gravity of the personal mobility system during movement according to the set action, and adjustment of the center of gravity is real-

ized via counterweight movement, which is controlled by the PID. The control system adjusts the center of gravity of the personal mobility system to the set value in 4 to 6 s. These observations indicate that the simulation results verify the feasibility and effectiveness of the proposed design.

## 4. Center of gravity self-adjustment experiment

### 4.1 Introduction of the physical experimental platform

The objective of this study was to verify the feasibility of the proposed design and the physical experiments used a 2.5-times reduced scale model. This smaller structure made the experiments more convenient and cost effective.

According to the moment formula, the product of the force on the front axis and the distance from the center of gravity to the front axis is equal to that of the force on the rear axis and the distance from the center of gravity to the rear axis. There-

fore, the distance from the center of gravity to the front axis in the experimental model  $y_{e1}$  is obtained as

$$y_{e1} = \frac{y_e F_{e2}}{(F_{e1} + F_{e2})} \quad (21)$$

where  $y_e$  is the distance from the front axis to the rear axis of the experimental model,  $F_{e1}$  is the force on the front axis of the experimental model,  $F_{e2}$  is the force on the rear axis of the experimental model, as shown in Fig. 8.

The weight of the target system is 15.625 times that of the experimental model and the actual size is 2.5 times that of the experimental model. Therefore, the distance from the center of gravity of the actual model to the front axis  $y_{a1}$  is

$$y_{a1} = \frac{2.5y_e * 15.625F_{e2}}{15.625(F_{e1} + F_{e2})} = 2.5 \frac{y_e F_{e2}}{(F_{e1} + F_{e2})} = 2.5y_{e1}. \quad (22)$$

This implies the actual center of gravity is 2.5 times the distance from front axis compared to that of the experimental

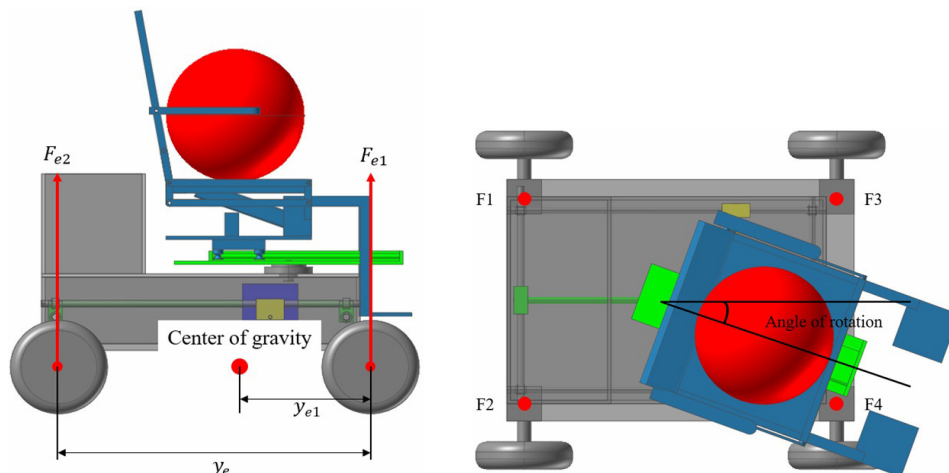


Fig. 8. Schematic diagram of the calculation of the center of gravity position.

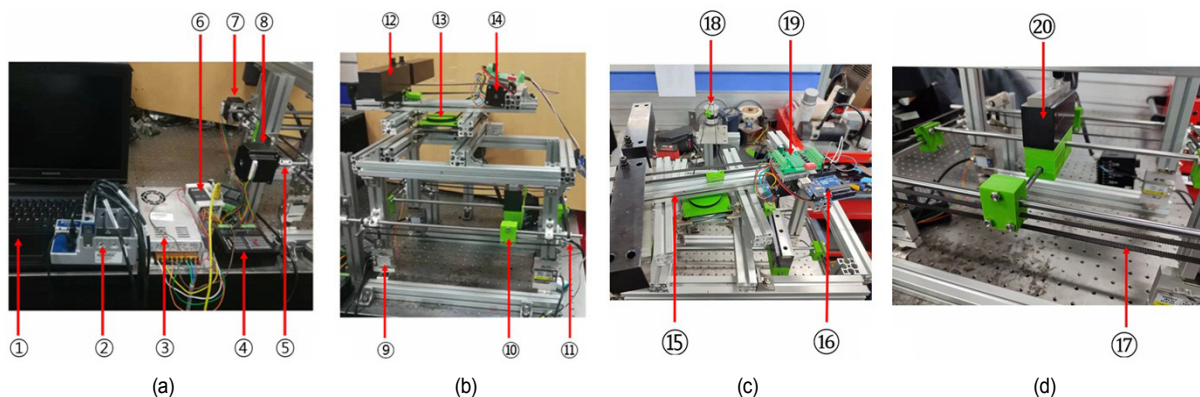


Fig. 9. Experimental bench (① laptop; ② NI cDAQ-9174 modules; ③ switching power supplies; ④ motor driver; ⑤ coupling; ⑥ PLC; ⑦ Y-axis motor; ⑧ X-axis motor; ⑨ load sensor; ⑩ slider; ⑪ pulley; ⑫ counterweight; ⑬ rotating structure; ⑭ servo motor to control seat advancement; ⑮ slide rail; ⑯ microcontroller; ⑰ belt; ⑱ stepper motor to control seat rotation; ⑲ motor driver; ⑳ counterweight that simulates the weight of the human body).

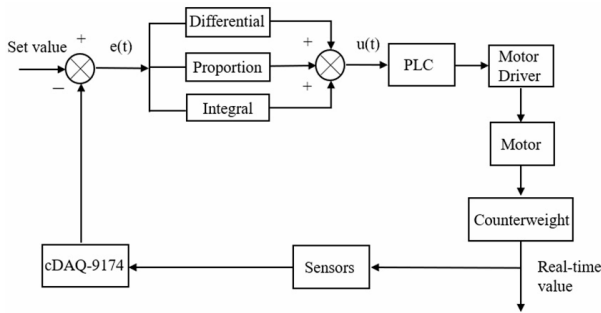


Fig. 10. Block diagram of control system.

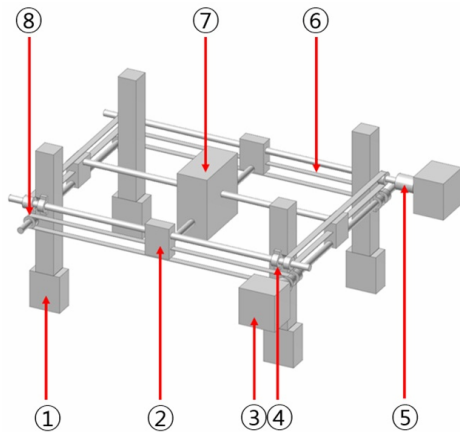


Fig. 11. Schematic diagram of the structure of the center of the gravity adjustment system (① load sensor; ② slider; ③ motor; ④ bearing block; ⑤ coupling; ⑥ belt; ⑦ counterweight; ⑧ pulley).

model. The experimental bench is presented in Fig. 9. A block diagram of the control system is shown in Fig. 10.

An NI cDAQ-9174 module and load sensor form the information acquisition module. A programmable logic controller (PLC) and motor driver are used as control modules. Stepper motor control along the X and Y axes is used for counterweight movement. The real-time center of gravity position is calculated based on real-time data from the four sensors and the initial center of gravity X- and Y-axis coordinates are used as the set values. The real-time center of gravity X- and Y-axis coordinates are used as the inputs and the pulse frequency of the motor is considered as the output. A schematic diagram of the structure of the center of gravity adjustment system is presented in Fig. 11.

The motor and peripheral shafts are fixed via coupling. The pulley is fixed to the peripheral shaft. The belt is fixed to the slider. The slider is fixed to the central shaft.

## 4.2 LabVIEW program

### 4.2.1 Modules for data acquisition

A block diagram of the LabVIEW program system is presented in Fig. 12. The functions of the data acquisition module (DAQ) include the following.

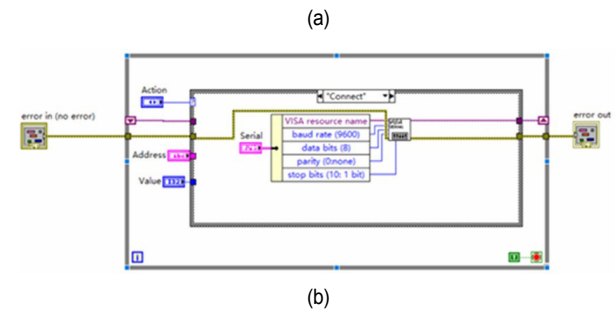
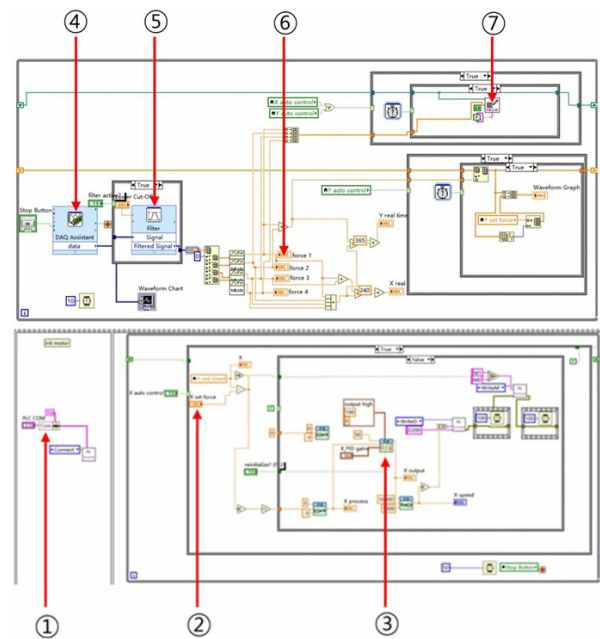


Fig. 12. Program diagram of LabVIEW: (a) block diagram of LabVIEW (① PLC communication function; ② set value module; ③ PID control unit; ④ DAQ; ⑤ filter; ⑥ center of gravity position calculation module; ⑦ data logging module); (b) program block diagram of the PLC.

1) Through the DAQ assistant, we can configure the acquisition hardware and channel information. We used the cDAQ-9174 chassis and NI cDAQ 9237 strain acquisition module. The signal input range was set to  $\pm 10$  v, the conversion unit was set to N, the measurement bridge type was set to the full bridge mode, the excitation power supply was set to internal excitation, the excitation voltage was set to 2.5 v, the resistance was set to  $350 \Omega$ , the acquisition mode was set to continuous acquisition, the sampling rate was set to 10000 according to the maximum signal frequency of 1000, and the number of sampling points was set to 2000.

2) The filtering method was low-pass filtering and the cutoff frequency was set to 100 Hz.

3) The filtered signal was converted into a two-dimensional array using a dynamic signal and the two-dimensional array was converted into a one-dimensional array with four channels. Then, an averaging process was performed to obtain the real-time values of the four forces.

4) After turning on the PID control mode, the data on the four channels were saved at regular intervals.



#### 4.2.2 Modules for data acquisition

This function block is referred to as function VI, which includes all operations on the PLC (e.g., the PLC connect, PLC write M, PLC write D, and disconnect operations).

1) Open the serial port and set the PLC serial port communication parameters, including the band rate, data bit, parity, and stop bit, which are set to 9600, 8, N, and 1, respectively.

2) Branch write M. Write the PLC M address, through which it can be set to the corresponding M value. For example, setting M2 to true means controlling the X-axis motor to stop.

3) Branch write D. Write the PLC D register through which the speed of different motors can be changed by changing the value of the register.

4) The branch is disconnected. When the branch is disconnected, the serial port closes and the program ends or exits.

#### 4.2.3 Program process in LabVIEW

The program process is to input the set value through the front panel and then make real-time comparative judgments based on the measured value and set value. If the set value is greater than the measured value, then the motor will drive forward. If the set value is less than the measured value, then the motor will be reversed. The direction of the motor is changed by setting M1 and M0 in the PLC. Additionally, the difference be-

tween the measured and set values is calculated to obtain K, which is converted into a percentage as an engineering unit for use as a PID input. Rotation through percentage engineering units determines the motor speed in pulses per second and the motor speed is changed by setting the D200 register in the PLC.

#### 4.3 Results of the experiment

In the first set of experiments, the seat rotation angles were 20°, 15°, and 10°. The forward distance of the seat was 120 mm and the forward speed of the seat was 80 mm/s.

Based on the results of the first group of experiments, Fig. 13 presents the motion curve of the center of gravity position of the personal mobility system along the X and Y axes. One can see that different rotation angles of the seat result in different vectors of seat displacement along the X and Y axes, leading to different times for the center of gravity self-adjustment system to complete center of gravity adjustment. Fig. 14 presents the load data measured by load sensors F1, F2, F3, and F4 during experimental test 1. The left-rear sensor is F1, right-rear sensor is F2, left-front sensor is F3, and right-front sensor is F4. Fig. 15 presents the variation curves of the X- and Y-axis motor pulse frequencies.

The second target variables was the forward speed of the

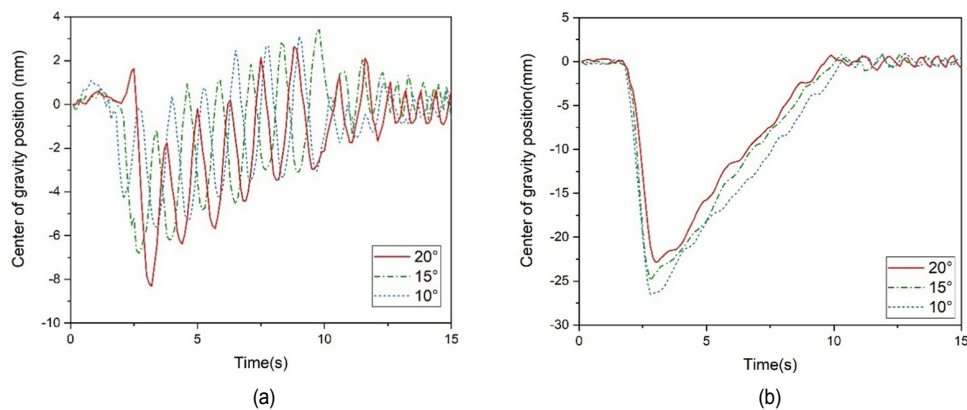


Fig. 13. Results of the center of gravity position in the experiments for different rotation angles of the seat: (a) movement along the X axis; (b) movement along the Y axis.

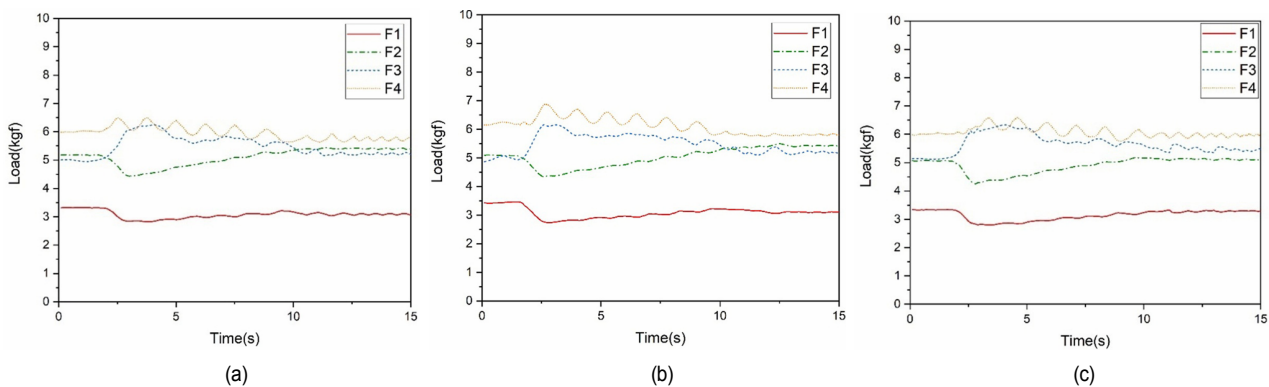


Fig. 14. Data from the load sensor for different rotation angles of the seat: (a) seat rotation of 20°; (b) seat rotation of 15°; (c) seat rotation of 10°.

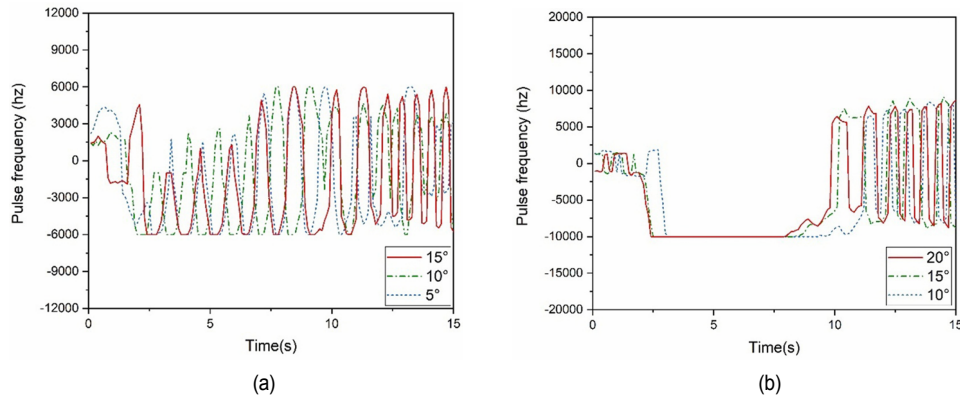


Fig. 15. Results of the center of gravity position in the experiments for different rotation angles of the seat: (a) X-axis motor pulse frequency; (b) Y-axis motor pulse frequency.

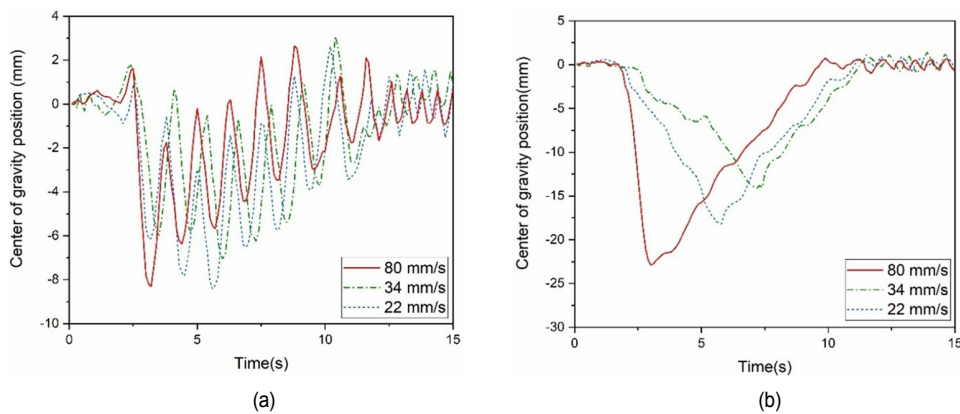


Fig. 16. Results of the motor pulse frequency in the simulations for different forward speeds of the seat: (a) movement along the X axis; (b) movement along the Y axis.

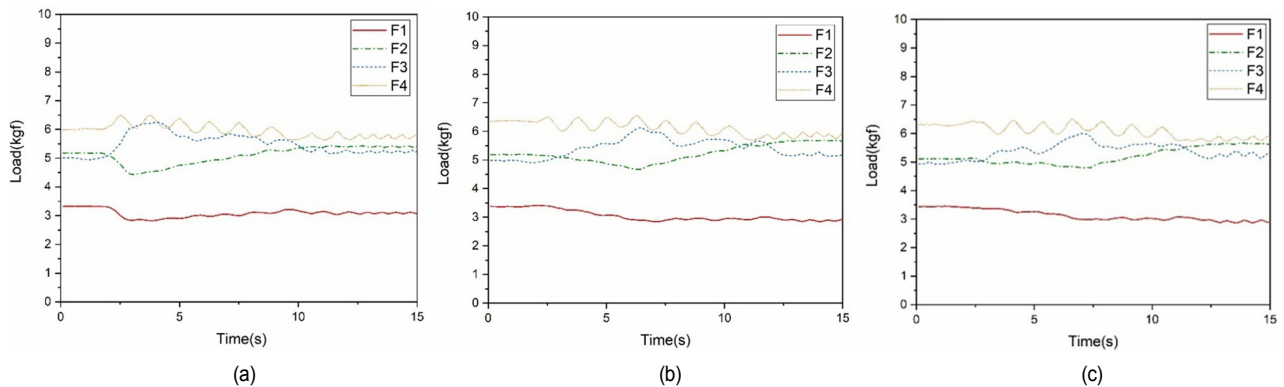


Fig. 17. Data from the load sensor for different forward speeds of the seat: (a) forward speed of 80 mm/s; (b) forward speed of 34 mm/s; (c) forward speed of 22 mm/s.

seat in the experimental test group with a rotation angle of  $20^\circ$ . The forward distance of the seat was fixed at 120 mm and the forward speed of the seat was 80, 34, and 22 mm/s.

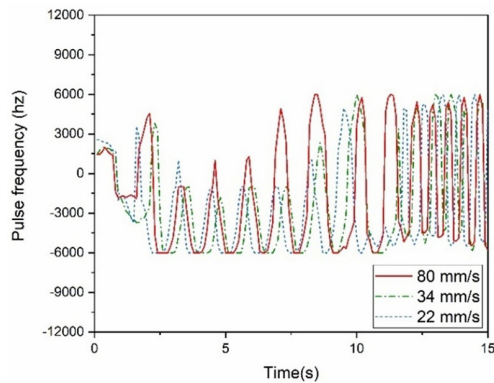
The results of the second group of experiments can be summarized as follows. Fig. 16 presents the movement curve of the center of gravity position of the personal mobility system along the X and Y axes, Fig. 17 presents the load data ac-

quired from load sensors F1, F2, F3, and F4 in experimental test 2. Fig. 18 presents the change curves along the X and Y axes for the motor pulse frequency.

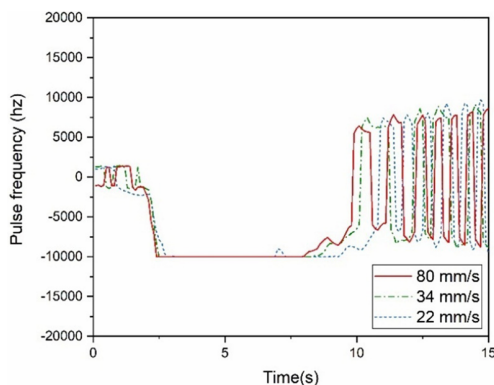
The PID control system quality index is the transition process curve index of the control system under the effects of a step-signal disturbance. The hardware and parameter settings of the control system affect its quality. The system is not meant to

Table 3. Quality indicators of the PID control system.

Seat advance speed (mm/s)	80
Seat advance distance (mm)	120
Seat rotation angle (degree)	20
Rise time (s)	7.8
Transition time (s)	10.8
Static difference (mm)	0.749
Overshoot (mm)	0.25
Attenuation degree	0.543
Oscillation period (s)	1.3



(a)



(b)

Fig. 18. Results of the motor pulse frequency in the simulations for different forward speeds of the seat: (a) X-axis motor pulse frequency; (b) Y-axis motor pulse frequency.

produce multiple groups of quality indicators under the interference of different step signals (i.e., different forward speeds and rotation angles of the seat). Therefore, only representative dataset was selected to produce a table to evaluate the control quality of the control system. Because the movement of the seat with a rotation angle of  $20^\circ$  and forward speed of 80 m/s leads to the most significant movement of the center of gravity, this experimental dataset was selected for the analysis of the quality indicators of the PID control system. The quality indicators of the PID control system used in the experiment are listed in Table 3.

The quality indicators of the PID control system are defined as follows.

#### 1) Rise time

The time at which the output quantity first reaches the set value indicates the speed at which deviations caused by disturbances are eliminated. This indicator describes the response speed of the system.

#### 2) Transition times

Time from the onset of a disturbance to the establishment of a new equilibrium state for the controlled quantity. This is an indicator of the transition process speed.

#### 3) Static difference

The static difference is the deviation from the set value at the end of the transition process or from the measured value in a follow-on system. The static difference represents the accuracy of the control system.

#### 4) Overshoot

Sometimes called the maximum deviation, this indicator represents the degree of deviation of a controlled value from a set value. This indicates the fluctuation of the transition process. A smaller fluctuation is desirable. The amount of overshoot is defined as:

$$\sigma_p = \frac{m_1}{S_V} \quad (23)$$

where  $m_1$  is the first wave peak,  $m_2$  is the second wave peak, and  $S_V$  is the set value.

#### 5) Degree of attenuation

The attenuation ratio is sometimes expressed in terms of the attenuation degree. The larger the decay ratio, the better the dynamic index of the transition time, which is defined as

$$\Psi = \frac{m_1 - m_2}{m_1 + S_V} \quad (24)$$

#### 6) Oscillation period

The time between the first and second wave crest of the transition process.

The center of gravity self-adjustment system adjusts the center of gravity of the personal mobility system to the set value over 7.8 s and with a static difference of 0.749 mm. According to the PID control system quality indicators, the center of gravity self-regulating PID control system designed in this study is stable, accurate, and fast.

### 4.4 Comparative analysis of simulation and experiment

The data for the rotation angle of  $20^\circ$  in the first group of simulations, for the rotation angle of  $20^\circ$  in the first group of experiments, and the simulation data for the rotation angle of  $20^\circ$  and forward speed of 80 mm/s without adding a speed limit were compared. The simulations without adding a speed limit

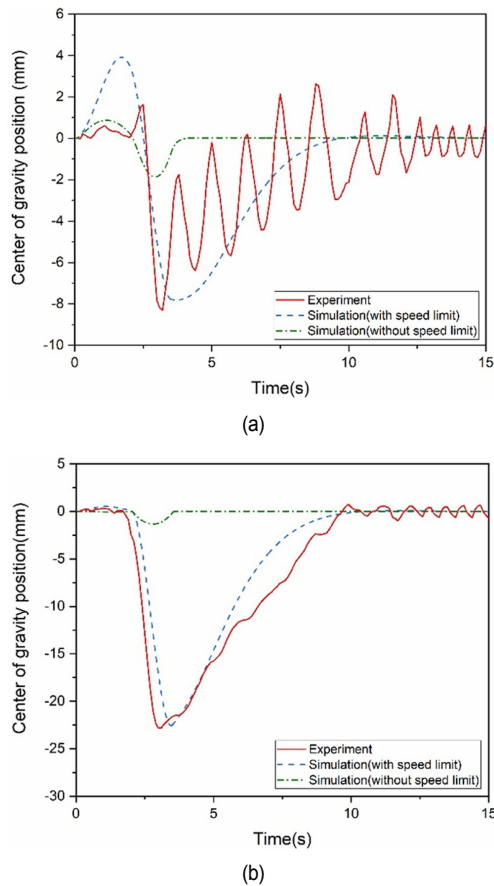


Fig. 19. Results of the center of gravity position in the experiments and simulations: (a) movement along the X axis; (b) movement along the Y axis.

were considered as the ideal condition and used as a reference when comparing data.

The experimental and simulation data are presented as graphs for comparison in Fig. 19.

The curves of the experimental and simulation results match within a certain error range. Both the experimental data and simulation results demonstrate that the designed personal mobility system for assisted agricultural work with a self-adjusting center of gravity is feasible. The center of gravity self-adjustment system implemented using PID control is effective.

## 5. Conclusions

In this study, a center of gravity adjustment system was designed to achieve the self-adjustment of the center of gravity of a personal mobility system. This study focused on the design and implementation of the center of gravity adjustment system to achieve self-adjustment of the center of gravity.

Based on the design of the personal mobile system, the center of gravity self-adjustment system is added to design a personal mobility system for assisted agricultural work with a self-adjusting center of gravity. The designed system can realize

the functions of automatic movement, seat rotation, forwarding, and changing posture, which can meet the mobility needs of disadvantaged people in daily life and agricultural activities.

The scaled-down 2.5 times 3D model of the system is established by multi-rigid body theory, and the model is simplified and divided into 7 parts according to Boolean operations so that the analysis obtained does not affect the simulation results and saves time and cost at the same time. The material of the simulation model is set, considering that the main structure of the personal mobility system belongs to various types of aluminum alloy. Because the seat part is set to wood and the tire is set to rubber, the other parts are set to aluminum alloy material type. After that, the multi-body dynamics analysis of the personal mobility system is carried out, and the differential equations of the system are obtained.

Constraints and drives are added to the simulation model, and a self-adjusting control method of the center of gravity based on the personal mobile system is established, with the initial center of gravity X-axis coordinates and Y-axis coordinates as input values, the center of gravity real-time X-axis coordinates and Y-axis coordinates as inputs, and the forces  $F_x$  and  $F_y$  applied to the counterweight as outputs. The PID control method is used, and the joint simulation by Simulink and multi-body dynamics software is used to conduct multiple simulation tests on the personal mobility system with seat rotation angle and forward speed as variables in the manned state.

An experimental model of the designed personal mobility system for assisted agricultural work with a self-adjusting center of gravity is constructed with an isometric reduction of 2.5 times compared to the actual size. A load sensor and a cDAQ-9174 module are used as the data acquisition module, a PLC and a motor driver are used as the control modules, and a stepper motor is used as the power source for counterweight motion in the X and Y-axis directions, respectively. The real-time center of gravity position is calculated based on the real-time data on the four sensors, and the initial center of gravity X-axis coordinates and Y-axis coordinates are used as the set values, the real-time center of gravity X-axis coordinates and Y-axis coordinates as input, and the pulse frequency of the motor as output. Similarly, several experimental tests are conducted on the personal mobility system under manned conditions with seat rotation angle and forward speed as variables.

The simulation results and experimental data demonstrate that the center of gravity self-adjustment system realized using PID control is effective and offers stability, accuracy, and speed. Therefore, the designed personal mobility system for assisted agricultural work with a self-adjusting center of gravity is feasible. The experimental transition time is 10.8 s and the simulated transition time is 10.4 s. The error between the two is 3.85 %, which is acceptable.

In previous related papers, personal mobility systems rarely have the adjustment of seat rotation and movement as in this thesis, as well as the use of force sensors to calculate the seat's center of gravity position.

## Acknowledgments

This work was supported by Inha University Research Grant.

## References

- [1] WHO, *Disability*, World Health Organization (2022) <https://www.who.int/en/news-room/fact-sheets/detail/disability-and-health>.
- [2] M. B. Warner, B. S. Mason, V. L. Goosey-Tolfrey and N. Webborn, Physical activity levels and shoulder pain in wheelchair users during COVID-19 restrictions, *Disability and Health Journal*, 15 (3) (2022) 101326.
- [3] E. D. Markus, T. Ntsinyi and E. Monacelli, Gesture recognition-based interaction with smartwatch and electric wheelchair for assistive mobility and navigation, *IOT with Smart Systems. Smart Innovation, Systems and Technologies*, Springer, Singapore (2022).
- [4] N. Prakash, E. Udayakumar and N. Kumareshan, Implementation of smart control of wheelchair for a disabled person, *Internet of Things and Its Applications*, EAI/Springer Innovations in Communication and Computing, Springer, Cham (2022).
- [5] S. Yamamuro, M. Hashimoto, S. Kato and K. Kuriyama, *Electric Wheelchair*, Patent No. US20070256872A1, US Patent and Trademark Office (2007).
- [6] P. M. Derasari and P. Sasikumar, Motorized wheelchair with bluetooth control and automatic obstacle avoidance, *Wireless Personal Communications*, 123 (2022) 2261-2282.
- [7] D. K. Kim, D. M. Kim, J. C. Park, S. G. Lee, J. Yoo and M. S. Lim, Torque ripple reduction of BLDC traction motor of electric wheelchair for ride comfort improvement, *Journal of Electrical Engineering and Technology*, 17 (2022) 351-360.
- [8] E. Yulianto, N. R. Munawaroh, T. Triwiyanto, P. C. Nugraha, Syaifudin, E. D. Setioningsih, T. Indrato and A. Kholiq, Obstacles and areas detection based on pulse width modulation method for electric wheelchair safety using ultrasound sensors, *Journal of Biomimetics, Biomaterials and Biomedical Engineering*, 50 (2021) 73-88.
- [9] M. Uemura, M. Sugimoto, R. Shimizu, N. Maeshige, Y. Yoshikawa and H. Fujino, The shift of the ischial region during maneuvering the standard wheelchair and the electric wheelchair in healthy adults, *International Journal of Clinical Medicine*, 12 (2021) 9.
- [10] J. W. Kim, Development of an autonomous driving smart wheelchair for the physically weak, *Applied Sciences*, 12 (1) (2022) 377.
- [11] H. R. Fajrin, T. A. Zain and M. Irfan, Design of electric wheelchair with joystick controller as personal mobility for disabled person, *Proceedings of the 1st International Conference on Electronics, Biomedical Engineering, and Health Informatics* (2021) 151-159.
- [12] A. Sasou, Acoustic head orientation estimation applied to powered wheelchair control, *2009 Second International Conference on Robot Communication and Coordination* (2009) 1-6.
- [13] H. A. Yanco, *Wheelesley: a robotic wheelchair system: indoor navigation and user interface*, *Assistive Technology and Artificial Intelligence* (1998) 256-268.
- [14] K. Choi and A. Cichocki, Control of a wheelchair by motor imagery in real time, *International Conference on Intelligent Data Engineering and Automated Learning*, Springer, Berlin, Heidelberg (2008) 330-337.
- [15] T. Shibata and T. Murakami, Power-assist control of pushing task by repulsive compliance control in electric wheelchair, *IEEE Transactions on Industrial Electronics*, 59 (1) (2012) 511-520.
- [16] Y. Heo, E. P. Hong, Y. H. Chang, B. Jeong and M. S. Mun, Experimental comparison of torque balance controllers for power-assisted wheelchair driving, *Measurement*, 120 (2018) 175-181.
- [17] H. Seki and A. Kiso, Disturbance road adaptive driving control of power-assisted wheelchair using fuzzy inference, *2011 Annual International Conference of the IEEE Engineering in Medicine and Biology Society* (2011) 1594-1599.
- [18] N. Tanohata and H. Seki, Comfortable driving control for electric power-assisted wheelchair on disturbance road using fuzzy algorithm, *2010 3rd IEEE RAS and EMBS International Conference on Biomedical Robotics and Biomechanics* (2010) 130-135.
- [19] H. Seki and N. Tanohata, Fuzzy control for electric power-assisted wheelchair driving on disturbance roads, *IEEE Transactions on Systems Man and Cybernetics Part C*, 42 (2012) 1624-1632.
- [20] S. Dubowsky et al., PAMM - a robotic aid to the elderly for mobility assistance and monitoring: a helping-hand for the elderly, *Proceedings 2000 ICRA. Millennium Conference, IEEE International Conference on Robotics and Automation* (2000) 570-576.
- [21] K. H. Han and C. H. Lee, A study on the development of personal mobility for the vulnerable group, *Journal of Drive and Control*, 18 (4) (2021) 35-42.
- [22] R. B. Bhat and R. V. Dukkipati, *Advanced Dynamics*, Alpha Science International, Oxford (2001).



**Zixuan Jiang** is a Master student in the Department of Mechanical Engineering, Inha University. He received his Bachelor of Science degree in 2019 from Mechanical Engineering, Qingdao University of Science & Technology. His research interests include control.



**Chul-Hee Lee** is a Professor in the School of Mechanical Engineering, Inha University. He received his Doctor of Philosophy degree in 2006 from Mechanical & Industrial Engineering, University of Illinois at Urbana-Champaign. He was a chassis research engineer at Hyundai Motor Co. from 1996 to 2002 and a senior research & development engineer at Caterpillar Inc. (USA) from 2006 to 2007. His research interests are in the areas of virtual product development by design optimization and FE analysis.